Catalysis Letters (2018) 148:1659–1675
https://doi.org/10.1007/s10562-018-2384-6

Investigation into Consecutive Reactions of Ethane and Ethene Under the OCM Reaction Conditions over Mn_xO_y–Na_2WO_4/SiO_2 Catalyst

Samira Parishan[1] · Ewa Nowicka[1] · Vinzenz Fleischer[1] · Christian Schulz[2] · Maria G. Colmenares[3] · Frank Rosowski[2] · Reinhard Schomäcker[1]

Received: 8 February 2018 / Accepted: 4 April 2018 / Published online: 18 April 2018

Abstract

The reaction mechanism of ethane and ethene oxidation was studied under the OCM reaction conditions over Mn_xO_y–Na_2WO_4/SiO_2. The consecutive reaction of C_2 components is observed to be the main route to the formation of CO_X under the applied reaction conditions here. The homogeneous or heterogeneous nature of these unselective reactions was investigated in more details. For this purpose, the temperature programmed surface reaction (TPSR) technique was applied. The results of these experiments indicate that the consecutive reaction of ethane is mainly occurring in the gas phase of the reactor. This point was confirmed when the activation energy of ethane both, in the presence of the catalyst and silicon carbide, as the inert surface, was shown to be at the same level. The concentration profile of the effluent obtained by simulating the reaction of C_2 components using the Dooley mechanism in ChemkinPro was also in good agreement with this proposal. The reason for the low influence of the catalyst on conversion of ethane was ascribed to the film diffusion limitation that is occurring under the OCM reaction conditions applied in these studies. Finally, a set of experiments were performed with $^{13}CH_4$ to study the effect of methane on the consecutive reaction of ethane in the OCM reactor.

Graphical Abstract

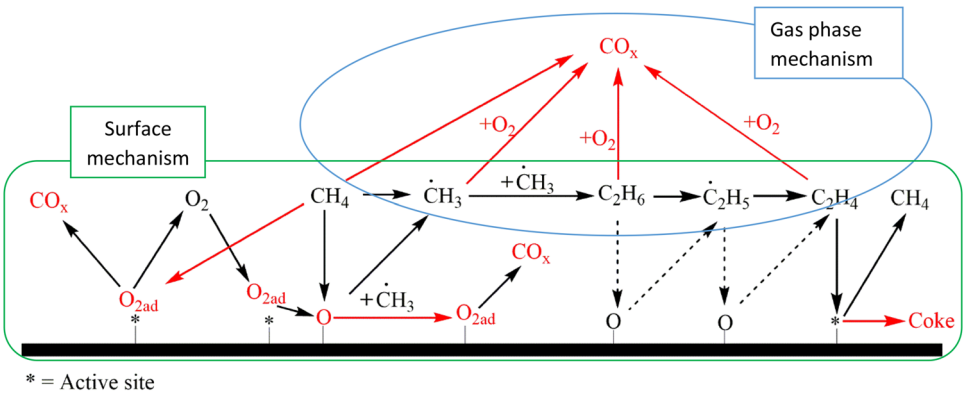

Keywords Oxidative coupling of methane · Mn_xO_y–Na_2WO_4/SiO_2 · Thermal dehydrogenation of ethane · Oxidative coupling of labelled methane · Stationary co-feeding experiments

1 Introduction

The large known resources of natural gas [1–4] as well as the volatile petroleum market and growing environmental concerns, attract an increasing attention to the processing of natural gas into value-added products (VAP) [5–9]. The

Electronic supplementary material The online version of this article (https://doi.org/10.1007/s10562-018-2384-6) contains supplementary material, which is available to authorized users.

✉ Reinhard Schomäcker
schomaecker@tu-berlin.de

Extended author information available on the last page of the article

conversion of methane to C_2 products and higher hydrocarbons, known as oxidative coupling of methane (OCM) (Eq. 1), could be a possible direct method for fulfilling this aim [3, 8, 10–12].

$$CH_4 + O_2 \rightarrow C_2H_6 \text{ or } C_2H_4 + 2\,H_2O \quad (1)$$

One of the advantages of this direct method for utilization of methane is that it is exothermic and therefore is not thermodynamically limited [3]. In addition, it represents the highest possible carbon efficiency of the converted methane compared to that of the other direct methods for conversion of methane to VAP [5]. However, despite all the research done on this process, it has not yet been commercialized, as the minimum yield of 30% towards C_2 products required to make this process economically viable, was not achieved.

The major reason for this limitation is the occurrence of side reactions which are thermodynamically more favorable and mainly lead to the production of carbon oxides. To improve the C_2 selectivity and yield of the process, it is essential to have a better control over the formation of unselective products. To reach that point, a good knowledge of the reaction mechanism and the origin of the formation of CO_X are essential. There is already a consensus that OCM follows a complex reaction network and carbon oxides are produced through both homogeneous and heterogeneous oxidation of its main hydrocarbons, i.e., methane, ethane, and ethene, see Fig. 1 [3, 6, 8, 11, 13–20]. Nevertheless, the total and partial oxidation of the C_2 components are reported based on isotope-labelled experiments to be the main routes for the production of CO_X [11, 21, 22]. Therefore, to enhance the reaction performance, the main focus should be on suppressing the oxidation of the ethane and ethene. The milestone to this aim is a detailed understanding of the mechanism of consecutive reactions of both these components. Investigating issues such as the contribution of the catalyst on their selective and unselective conversion should reveal more details.

In the literature, the mechanistic studies are carried out mostly by tracing the reaction of methane. Under these circumstances, the conversion of C_2 components take place both in sequence and parallel to the direct conversion of methane. In Fig. 1 the status of the discussion of the OCM mechanism is summarized [3–23]. Therefore, the results of the methane coupling reaction do not provide sufficient information about the mechanism of ethane and ethene consecutive reactions.

To solve this problem, we investigated the reaction of ethane and ethene separately from methane, but under the conditions close to OCM. First, the temperature programmed surface reaction (TPSR), co-feeding and isotope-labelled experiments were conducted to study the reaction network of C_2 components. Then, the experimental observations were verified by simulating the reaction of ethane and ethene in Chemkin Pro. Finally, in ^{13}C methane isotope labelled experiments the influence of methane on the consecutive reaction of C_2 components was compared with the conditions applied in our tests without methane. The Mn_xO_y–Na_2WO_4/SiO_2, which is already known as one of the most stable and best-performing catalysts for OCM, [1, 3, 8, 23, 24] was chosen as the model catalyst in these studies.

2 Experimental Section

2.1 Catalyst Preparation

All catalytic reactions were performed using a Mn_XO_Y–Na_2WO_4/SiO_2 catalyst. This material was chosen as the model catalyst based on the previous reports documenting it as one of the most efficient and stable catalysts

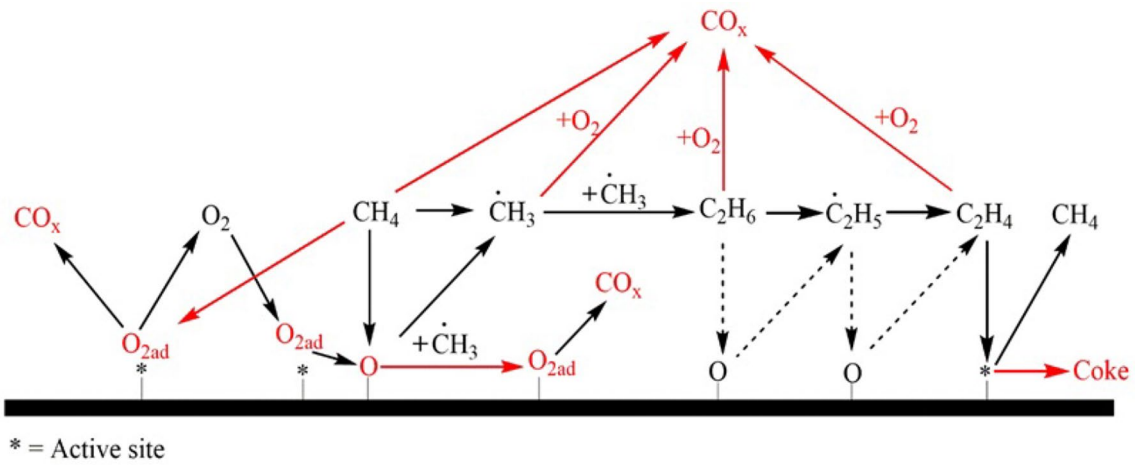

Fig. 1 Simplified reaction network of OCM

for OCM [3, 20, 25–27]. The material was prepared by incipient wetness impregnation as described by Fang et al. [28]. First, amorphous SiO_2 (Silica Gel, Davisil, Grade 636, Sigma-Aldrich) was sieved to the particles diameter of 200–350 µm, and impregnated in two steps using aqueous solutions of $Mn(NO_3)_2{\cdot}4H_2O$ (p.a.,≥ 97%, Sigma–Aldrich) and $Na_2WO_4{\cdot}2H_2O$ (p.a.,≥ 99%, Sigma-Aldrich) in adequate concentration. After each impregnation step, the sample was dried in a cabinet dryer at 100 °C, overnight. The obtained solid was then calcined at 800 °C for 8 h under static air. An annealing procedure was performed using a heating rate of 1 K/min. The final catalyst was none porous and had a specific surface area of 3.2 m^2/g. It consists of 5 wt% Na_2WO_4 and 2 wt% Mn(II) on SiO_2.

2.2 Feed Gases

Methane (99.95%), ethane (99.95%), ethene (99.90%), oxygen (99.998%) and helium (99.999%) were purchased from Air Liquide. The pure labelled methane ($^{13}CH_4$ 99 atom % ^{13}C) was provided by Sigma Aldrich. All the gases were used in the experiments as received, without further purification.

2.3 Reactor Setup

A simplified scheme of the experimental setup is presented in Fig. 2. The dashed line shows the path of the effluent in the isotope-labelled experiments. In all the other experiments the gas stream goes directly to the analytical instrument as presented by the solid line.

Unless noted, all the catalytic and blank tests are performed using 1 g of the solid material sieved in the range of 200–300 µm. Two reactors which were different in geometry, but both made of quartz were used in our studies. These reactors were located in a temperature controlled oven (T range 25–900 °C). The temperature in the catalytic bed was measured using a type K thermocouple. To regulate the flow of the gasses, Mass Flow Controllers (EL-FLOW, Bronkhorst) were used. To ensure a homogeneous reaction mixture a mixing cylinder was built before the reactor inlet. The pre-catalytic pressure was monitored using the P-I-1, the pressure indicator 1. Depending on the experiment, either the mass spectrometer (MS), the gas chromatograph (GC) or the MS attached to a GC column were employed to analyse the composition

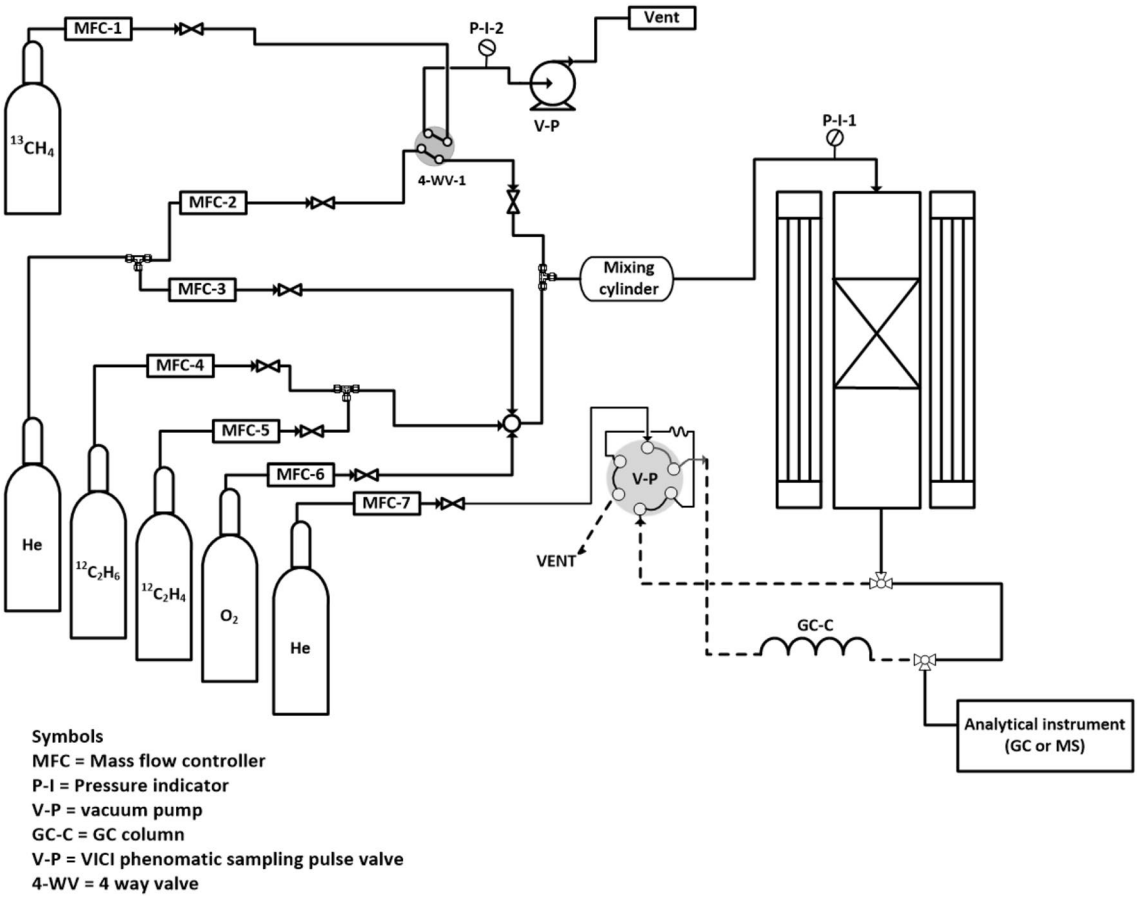

Fig. 2 Schematic of the experimental setup

of the effluent. Nevertheless, both the GC and MS were calibrated to distinguish alkanes and alkenes of C_{1-3} as well as CO, CO_2, N_2, and O_2. Since helium was used as the carrier gas of the GC, neither H_2 nor He could be detected by GC, however, this limitation does not apply to the measurements done with the MS.

Unless otherwise mentioned, all the tests were performed in a tubular fixed-bed reactor with 9 mm internal diameter i.d and 35 cm length. A quartz frit with the pore size of 120 µm, was placed in the middle of this reactor to keep the catalyst in its position. This set up was equipped with a quadrupole mass spectrometer (Inprocess Instruments GAM 200) [29].

Kinetic investigations were conducted in a U-shaped fixed-bed reactor with 6 mm i.d and 25 cm length. The total flow and the volumetric flow of hydrocarbon in the reaction mixture were kept constant in these experiments. However, the concentration of oxygen was varied by substituting it with the same flow of the inert gas. The reaction performance was calculated in a temperature range of 570–630 °C. To measure the composition of effluent with a high accuracy, an Agilent GC (7890 A) was used for gas analyses. The GC was equipped with a flame ionization detector (FID) and a thermal conductivity detector (TCD). The separation of effluent was done in a HP-PLOT/Q and a HP Molsieve column. As mentioned earlier, the GC carrier gas was He (Air Liquide, purity 99.999%) therefore the detection of H_2 and He was not possible in these experiments [30].

For the isotope-labelled experiments, the post and pre catalyst sections of the tubular reactor were modified. The experiments were performed using a mixture of $^{13}CH_4$ and $^{12}C_2H_6$ hydrocarbons. The total flow of the reaction mixture was fixed at 70 Nml/min. The volumetric flow of methane was changed from 0 to 5 Nml/min by substituting its flow by the inert gas. A vacuum pump was installed on the set up to purge all the lines connected to the bottle of the labeled gas. The effluent was consisting of a range of products with overlapping ionic masses such as CO, C_2H_4, C_2H_6 and their isotopes. Therefore, for reliable analytical results, the gas components were separated, before entering the MS. For this purpose a Hayesep Q column of Agilent was installed at the inlet of the mass spectrometer. The effluent was sent to a VICI pneumatic sampling pulse valve with helium as the carrier gas, see Fig. 2. To ensure that the investigations are carried out under steady-state conditions, the effluent was injected to the analytical instrument at least 5 min after the reaction started. More details regarding the construction of the set up, in addition to the calibration and measurement methods applied in these experiments are provided elsewhere [31–33].

3 Methods and Experiments

3.1 Temperature Programmed Surface Reaction (TPSR)

To distinguish between the catalytic and non-catalytic consecutive reactions of C_2 components from each other, the temperature programmed surface reaction (TPSR) technique was implemented. These experiments were conducted either by using 0.5 g of the catalyst or equal volume of an inert bed (quartz sand or silicon carbide). The first step in each of these experiments consisted of surface oxidation at 820 °C under a flow of 40 Nml/min of He and O_2 at a ratio of 1 to 1. Then, the temperature was decreased to room temperature under the same reaction flow. At the end, the bed was heated with a ramp of 1 K/min to 800 °C; while, a flow of 30 Nml/min of 5% ethane or ethene diluted with He was passing through the reactor. The catalyst was kept at 800 °C for 10 min before it was cooled down under the same reaction flow to room temperature with a ramp of 1 K/min. The changes in the composition of effluent were continuously recorded by the mass spectrometer and the results were presented as a function of the catalyst bed temperature.

3.2 Mechanistic Studies in Stationary Co-feeding Mode

A total flow of 70 Nml/min of either C_2H_6/O_2/He or C_2H_4/O_2/He (volume ratio1/1/33) was used as the feed. The reason for working with highly diluted gas mixture was to mimic the concentration ratio of C_2 components formed during OCM. To distinguish the surface reactions from those occurring in the gas phase one catalytic and two blank co-feeding experiments were performed. The first blank experiment was conducted in the empty reactor and the second was carried out in the presence of SiC (particle size 200–300 µm) as the inert surface. The amount of SiC in the later condition was set in a way that it provides the same volume as 1 g catalyst. However, the total flow in the former study was raised to 175 Nml/min to compensate the changes in the residence time caused by the removal of fixed bed. All the other reaction conditions applied in the catalytic and blank experiments were kept identical in these experiments. The oven was heated with a rate of 1 K/min to a maximum temperature of 750 °C. To ensure a constant flow during the heating of catalyst bed, the reaction mixture was introduced to the reactor at least 2 h prior to turning the oven on.

3.3 Kinetic Studies in Stationary Co-feeding Mode

These studies were performed to measure the activation energy and the reaction order of oxygen for the consecutive reaction of ethane. The first investigations were done in the presence of 1 g of the catalyst while the blank experiments were conducted using SiC. The amount of SiC was set in a way that its volume would be equal to the volume of 1 g of the catalyst. These experiments were performed in the U-shaped reactor connected to the GC. The total flow was set at 90 Nml/min throughout the whole experiment. The reaction mixture was consisting of a fixed amount of C_2H_6 (25 Nml/min) while the volumetric flow of oxygen varied between 0, 3, 4, 5, 6, 7 Nml/min. The reaction performance was measured for each of the described reaction mixtures at the temperature range of 585, 600, 615 and 630 °C, in the catalytic experiment, and at 585, 600, 615, 630 and 645 °C, in the blank tests.

3.4 Experiments with ^{13}C Labelled Methane

For this experiment, 1 g of the catalyst was placed in the isothermal zone of the fixed bed reactor. To keep the residence time constant the total flow, 70 Nml/min, was kept constant for the extent of the experiment. First, the catalyst was heated under the flow of He to 700 °C with a temperature ramp of 10 K/min. As soon as the target temperature was established the gas composition was switched from He to a mixture of 3/3/64 Nml/min of C_2H_6/O_2/He. The helium flow was divided between two different flow controllers, MFC-2 and MFC-3, which were set at 5 and 59 Nml/min respectively. The reason for this was to ensure continuous flow in the line connecting the 4-WV-1 (4 way valve-1, Fig. 1) to the reactor when the flow of methane was switched off. Otherwise, either back mixing or dead volume could have been created in these lines and falsify the experimental results.

In the next step, labeled methane was added to the earlier reaction mixture by switching the flow from 5 Nml/min of helium to $^{13}CH_4$. The MFC-1 (used for dosing methane) was set at 5 Nml/min before the direction of the valve was changed. The gas composition of 3/3/59/5 Nml/min of C_2H_6/O_2/He/$^{13}CH_4$ was sent to the reactor. All the other reaction conditions were kept constant. The changes in the composition ratio of effluent were continuously recorded by the MS.

To improve the accuracy of the analyses, the post-reactor section of the set up was modified to operate as a GC–MS. The effluent was sent to the sampling loop of a VICI pneumatic pulse valve which used 10 Nml/min of helium as the carrier gas. A GC Hayesep Q column was installed between the pulse valve and the MS. The carrier gas was passing through the column creating the baseline in the MS. For measurements, the valve was switched toward the sampling loop, where the carrier gas could take the reaction sample to the analyzer. The gas species in the reaction mixture were first separated by the GC column, before entering the MS. Since, the CO, O_2, and CH_4 could not adsorb on the Hayesep Q column, they were detected at the same time shortly after the injection. This was followed by the detection of the well-separated peaks of CO_2, C_2H_4, and C_2H_6 one after the other. To calculate the concentration of the isotopes of each of the components, the changes in the ion intensity of a specific ionic mass at the corresponding residence time of the component was put into consideration, see Table 1. The first measurements were conducted at least 30 min after each of the reaction conditions were established. A 15 min time interval was applied between every two measurements, conducted under the same reaction conditions.

3.5 Design of the Experiments

The consecutive reaction of ethane and ethene in the OCM reactor is assumed to be taking place on both the catalyst surface and in the gas phase [22, 23, 34]. Under these circumstances, investigating the reaction mechanism of these components is quite difficult. First, to decrease the complexity of these studies, the latter reactions were distinguished from that of the former one by applying the TPSR technique [34]. This technique is quite informative in studying the reaction mechanism of the selective oxidation reactions, especially those which are taking place over a catalyst capable of either storing oxygen, similar to our catalyst [23, 35], or providing its bulk oxygen.

In the next step, the conversion of ethane and ethene in the presence of gas phase oxygen, i.e., in the co-feeding mode, was analyzed. The purpose of these experiments was to study the phenomena observed in the TPSR experiments more in detail. Furthermore, the influence of the gas phase mechanism on the reaction network of C_2 components was surveyed. The condition of the catalyst pore and film diffusion limitation in these experiments were determined by calculating the Weisz–Prater and Mears criterion parameters.

Further, the kinetic parameters for the reaction of ethane were measured to examine the accuracy of the mechanistic studies. The conversion of C_2 components, under the experimental conditions applied in the co-feeding experiments was

Table 1 The ionic masses considered to quantify the isotopes at the residence time specified for each of the components

Component	^{12}CO	^{13}CO	$^{12}CO_2$	$^{13}CO_2$	$^{12}C_2H_4$	$^{13}CH_2CH_2$	$^{13}C_2H_4$	$^{12}C_2H_6$	$^{13}CH_3CH_3$	$^{13}C_2H_6$
Ionic mass	28	29	44	45	25	29	30	25	31	32

verified by simulating these reactions in Chemkin-Pro. To conduct the simulation, Dooley's mechanism [36, 37], which was shown to be the best available microkinetic model, presenting the gas phase reactions of the OCM process [38], was implemented.

Finally, the influence of methane on the reactions of C_2 components was studied by adding labelled methane to the reaction mixture.

4 Results and Discussion

4.1 Origin of the Secondary Oxidation of C_2 Components

As the literature studies show, the consecutive reaction of C_2 components is the main pathway towards the formation of carbon oxides in the OCM reactor [11, 21, 22]. The same conclusion was made from a series of co-feeding experiments conducted in this study. A flow of 70 Nml/min of CH_4/O_2/He, C_2H_6/O_2/He or C_2H_4/O_2/He with the ratios of 4/1/5, 1/1/33 and 1/1/33, respectively, were fed to the reactor loaded with the catalyst. The former reaction mixture (CH_4/O_2/He at the ratio of 4/1/5) was the standard gas composition ratio used to investigate the OCM reaction, while the latter two were set to mimic the real concentration of C_2 components formed during OCM. The performance of the reaction of each of these gas mixtures was calculated at 750 °C and considered as the base of our analysis. As the results in Table 2 show, conversion of both ethane and ethene, despite their high dilution has resulted in a significantly higher yield of carbon oxides in comparison to the experiment performed with the OCM standard gas composition. As shown in Table 2, CO is the main unselective reaction product in oxidation of ethane and ethene. This is very different from methane which resulted in formation of CO_2 as main unselective products. This difference in product distribution can be related to the initial concentration of molecular oxygen in C_2 co-feeding experiment (O_2:C_2H_X:He ratio of 1:1:33) that is lower than in the normal OCM reaction mixture (O_2:CH_4:He ratio of 1:4:4). As shown in Fig S5 CO_2 is the main carbon oxide product in the reaction using ethene. This trend is sustained as long as the concentration of oxygen remains relatively high. Once almost all oxygen is consumed (temperature around 700 °C) the concentration of CO continuously increases with reaction temperature while that of CO_2 decreases. The outcome of this experiments as well as results obtained in the TPSR experiments suggest CO as the primary product of the unselective oxidation of ethene. If enough oxygen would be available in the reactor (e.g. like in the standard OCM reaction), then CO will be further oxidized to CO_2. The difference in the nature of the main carbon oxide product observed in our studies (CO) and in the literature reports (CO_2) is then further explained by the reaction mechanism. This observation is in good agreement with the literature studies where the C_2 components are reported to have a higher reaction rate for total oxidation reactions than methane [22, 39–41]. Based on these results, it is concluded that the secondary oxidation of ethane and ethene is the main route towards the production of undesired products in the presence of Mn_xO_y–Na_2WO_4/SiO_2 catalyst, as well.

When the consecutive reaction of C_2 components was identified as the main pathway towards the production of carbon oxides in the OCM reactor, the mechanism of formation of these unselective products became a matter of investigation. As it was mentioned earlier, the reaction of OCM is accepted to take place both homo- and heterogeneously [3, 5, 13, 42]. First, the heterogeneous mechanism was studied separately from the homogenous part by implementing the TPSR technique [43].

Two sets of experiments were conducted with either ethane or ethene as the reactant. The investigations were done in the presence of the catalyst, quartz sand, and silicon carbide, sequentially. The latter two materials were used as an inert surface to perform the blank experiments. In each of the experiments, the surface was firstly oxidized under a flow of O_2 at 820 °C for 30 min. Then, the reactor was cooled down to room temperature under the same reaction flow. Finally, the surface was heated slowly (1 K/min) to 800 °C under a flow of either ethane or ethene, which were diluted with He. The changes in the composition of effluent were continuously recorded with the mass spectrometer. The results of the catalytic experiments are presented as a

Table 2 The performance of the reaction using CH_4 : O_2 : He = 4:1:5, C_2H_6 : O_2 : He = 1:1:33, and C_2H_4 : O_2 : He = 1:1:33 at 750 °C, total flow 70 Nml/min (using 1 g Mn_xO_y–Na_2WO_4/SiO_2 catalyst)

	$X(C_XH_Y)$	$S(C_2H_6)$	$S(C_2H_4)$	$S(CO_2)$	S(CO)	$Y(C_{2+})^a$	$Y(CO_X)$
CH_4 : O_2 : He	19.45	25.47	34.48	34.89	0.7	12.72	6.92
C_2H_6 : O_2 : He	94.57	–	50.34	2.9	35.8	50.22	36.58
C_2H_4 : O_2 : He	47.96	2.9	–	6.91	74.15	3.65	38.88

[a](C_2^+) in the experiment carried out using ethane is defined to be the sum of C_2H_4, C_3H_8, and C_3H_6, while that in the experiments with ethene includes the latter two hydrocarbons plus formed C_2H_6

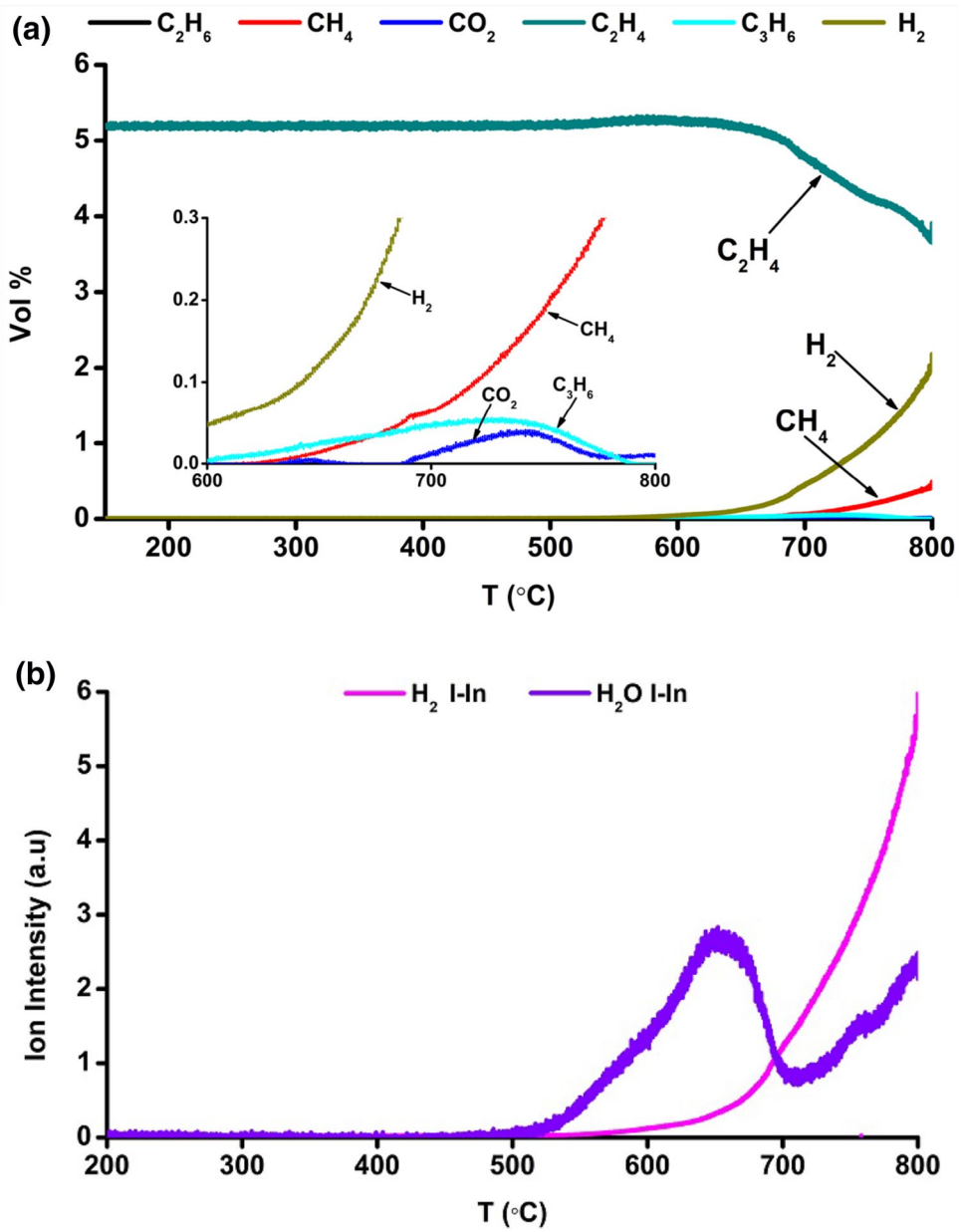

Fig. 3 Results of the TPSR experiment with ethene, **a** composition ratio of effluent, **b** nominal ion intensity of the water and H_2 in the reactor outlet vs. the temperature of the catalytic bed. Catalyst amount = 0.5 g, C_2H_4:He = 1:19 and total flow = 30 Nml/min

function of the temperature in Figs. 3 and 4. The reaction behavior in these experiments was compared with the stationary co-feeding ones (SI, Figure S5 and S7). With these experiments, not only some characteristics of the reaction mechanism of C_2 components were revealed, but also the origin of their secondary oxidation was clarified as discussed in the following paragraph.

In the ethene TPSR experiments, a continuous increase in the carbon balance was observed with the reaction temperature (SI, Figure S8). The raise was simultaneous with the detection of hydrogen as the main product of the reaction (Fig. 3a). This observation was assigned to the high tendency of ethene to decompose (reaction 2) under the applied reaction conditions [40, 44–46]. The decomposition of ethene is proposed to take place mostly over the catalyst surface since the rate of conversion in the blank TPSR experiment (SI, Figure S9) was not comparable to the catalytic one. In contrast to the TPSR experiments, where coke was the main reaction product, in the co-feeding experiment mostly carbon monoxide was formed (see SI, Figure S5). The level of conversion in the TPSR experiments was several times lower than in the co-feeding one. Therefore, the formation of CO_X in the latter experiment is assigned to both the oxidation of coke (the product of ethene decomposition reaction) and the direct oxidation of ethene.

It is worth emphasizing that the chance of selective reaction of ethene and oxygen to form VAP is higher over the catalyst surface than in the gas phase [47]. But even on the

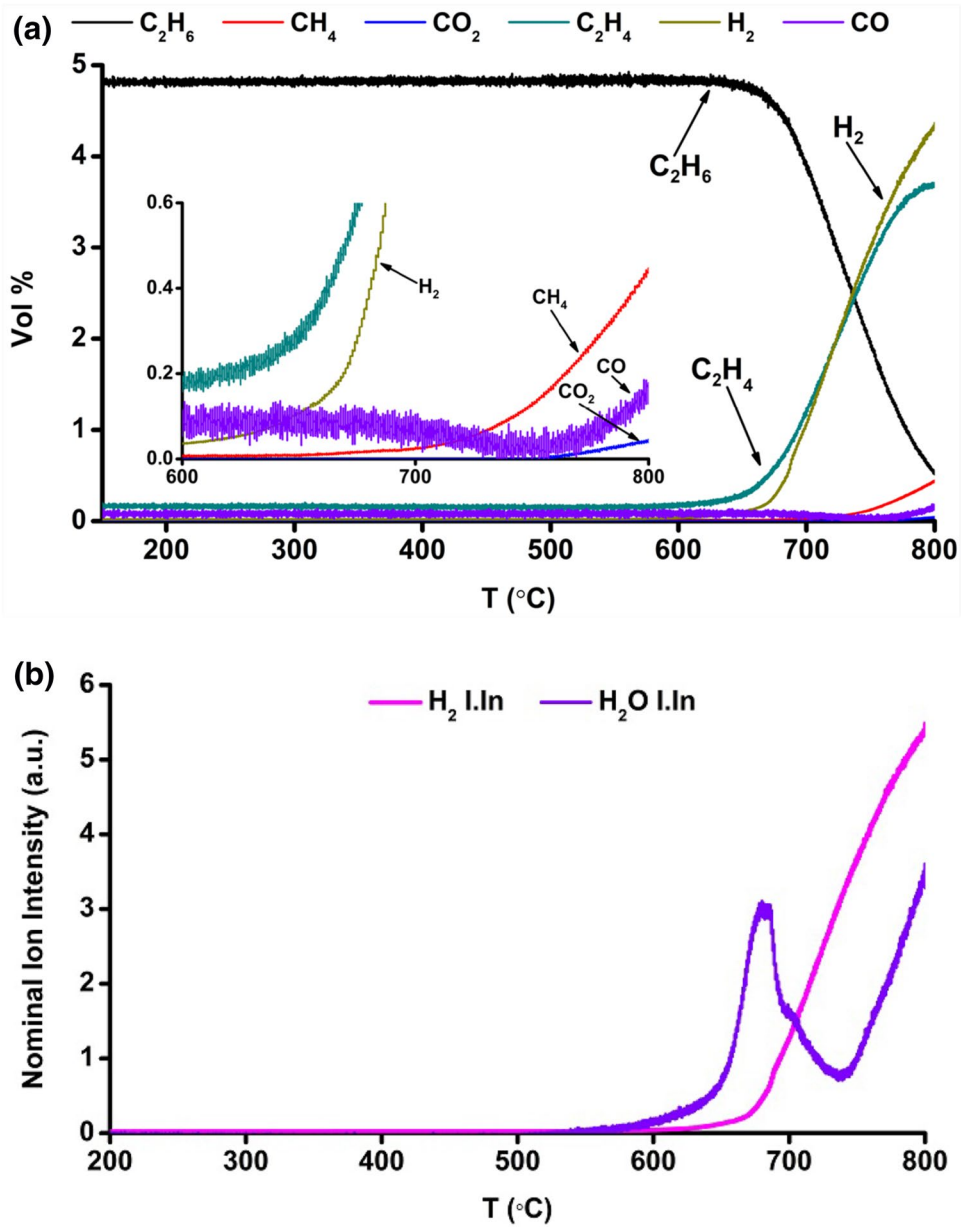

Fig. 4 Results of the TPSR experiment with ethane, **a** composition ratio of effluent, **b** nominal ion intensity of the water and H_2 in the reactor outlet vs. the temperature of the catalytic bed. Catalyst amount = 0.5 g, C_2H_6:He = 1:19 and total flow = 30 Nml/min

surface, oxygen forms either electrophilic or nucleophilic species [48]. At the high temperature of OCM, both these oxygen species convert ethene unselectively to CO_x products. The nucleophilic species cleave the C-H bond in ethene and form unstable and highly active radicals. These radicals are then over-oxidize in the presence of gas phase oxygen either directly or after forming higher chain hydrocarbons. Moreover, there is a high chance for the collision of radical intermediates to any available surface which results in the formation of coke. On the other side, the electrophilic oxygen would attack the C–C double bond in ethene and forms the epoxies which quickly convert to deep oxidation products at OCM temperature. Therefore, as observed in these studies and reported in the literature [11, 39, 49], the possibility of selective conversion of this component under the harsh reaction conditions of OCM, is always low.

In a second TPSR experiment, ethane was employed as a substrate (Fig. 4). As it is shown in Fig. 4a, ethane starts to react at around 600 °C and produces ethene as expected [13, 49–52]. However, the general assumption is that this conversion occurs by dehydrogenation of ethane with the active oxygen species at the catalyst surface. This reaction is known as oxidative dehydrogenation (ODH) and is presented by Eq. (3) [13, 17, 27, 42, 53]. However, simultaneous detection of hydrogen and ethene at a molar ratio of one to one in our experiment (see Fig. 4a), proposed the thermal dehydrogenation (TDH), presented in Eq. (4), as the main route for this conversion. The pattern of hydrogen and ethene formation

remained identical until the temperature of the catalyst bed exceeded 750 °C. When the concentration of formed ethene and the reaction temperature increased the rate of the ethene decomposition reaction also increases. Therefore, the concentration of hydrogen exceeds that of ethene during this period of the reaction. The proposed TDH reaction was confirmed by observing an identical product pattern during the cooling as well as along the heating period (SI, Figure S10 and S11).

In the next step, the catalytic or non-catalytic nature of TDH reaction of ethane was surveyed. To do so, the catalyst bed was substituted by either quartz sand or silicon carbide and the ethane TPSR experiment was repeated. The reaction performance was calculated for each of these experiments and the results were presented in comparison with each other in Fig. 5. The level of conversion in the blank experiments (performed over the SiC and quartz) was equal to that in the catalytic test. Therefore, it was concluded that the TDH of ethane is not a catalytic reaction.

It was also shown that the occurrence of the TDH reaction in the gas phase has no thermodynamic constraints under the OCM reaction conditions. This is because, a negative free enthalpy was calculated for this reaction at temperatures higher than 400 °C using the thermodynamic data reported by Deutschmann [54].

$$C_2H_4 + 2^* \rightarrow 2C^* + 2H_2 \quad (2)$$

$$C_2H_6 + O^* \xrightarrow{ODH} C_2H_4 + H_2O^* \quad (3)$$

$$C_2H_6 \overset{TDH}{\longleftrightarrow} C_2H_4 + H_2 \quad (4)$$

$$\Delta G = -RTln\ K_x \quad (5)$$

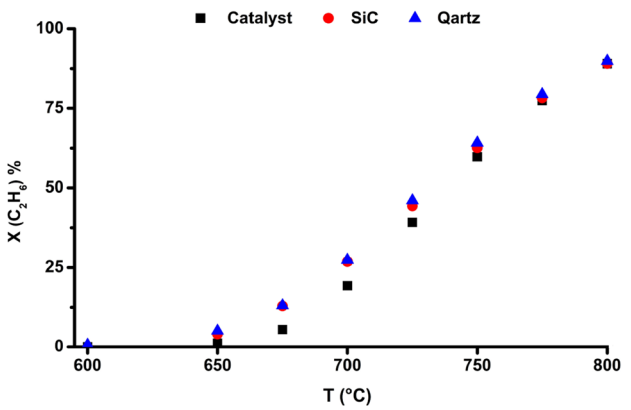

Fig. 5 The conversion of ethane as a function of the reactor temperature obtained in the TPSR experiments conducted over catalyst (filled square), silicon carbide (red colored circle), quartz (filled triangle), C_2H_6:He ratio of 1:19 at a total flow of 30 Nml/min, heating rate 1 K/min

The possibility of TDH reaction as the main route for converting ethane under the studied experimental conditions was confirmed by comparison of the theoretical and experimental conversion. An equilibrium constant (K_x) of 2.14 was calculated for the TDH of ethane under the applied reaction conditions at 750 °C. For this purpose, Eq. (5) was used. This value of K_X corresponds to a theoretical conversion of around 67% which correlates well with the experimentally measured value of 77%. The 10% difference between the experimental and theoretical conversions reported here is assigned to the occurrence of less dominating reactions such as oxidative dehydrogenation (ODH), unselective oxidation or coke formation reactions.

Based on all these evidence, the TDH of ethane was assumed as the main reaction for producing ethene under the applied reaction conditions here. This reaction is also shown to be mostly taking place in the gas phase of the reactor as reported in the earlier studies, too [52, 55]. Besides, these mechanistic interpretations are in accordance with the literature observations, where the rate of formation of ethene is shown to be independent of the concentration of surface active oxygen ([56]) and the type of catalyst [57].

Another important observation made in the TPSR experiments was related to the lower rate of CO_X formation (see Figs. 3a, 4a) in comparison to the co-feeding tests (SI, Figure S5 and S7). It is worth mentioning that the most important difference between the former and the latter experiments was the absence of the molecular gas phase oxygen in the reactor. Therefore, this behavior is assigned to the high contribution of gas phase reactions to the rate of secondary oxidation of the C_2 components. Accepting this point would have a drastic influence on the choice of the reaction techniques leading to an improvement in the performance of OCM. Therefore, this idea was studied in more details experimentally as well as by conducting simulations.

The experimental studies were conducted by studying the reaction of ethane and ethene in two different blank co-feeding experiments. The details regarding the reaction conditions applied in each of these experiments (in empty reactor and using SiC) are explained in detail in the experimental section. The results of the reaction performance obtained in these experiments are presented in comparison to the catalytic test in Fig. 6. As shown, the reaction performance obtained in these three studies were almost identical. It should be noted that the experiment conducted in the presence of the SiC was performed with a time delay of about 1 year from the other two studies. Therefore, the differences observed in its performance from the latter two tests are suggested to be mostly related to the variations occuring in the set points of the set up such as calibration factors of both the mass flow controllers and the mass spectrometer. However, the small differences observed in the conversion and selectivity of the catalytic reaction with the one

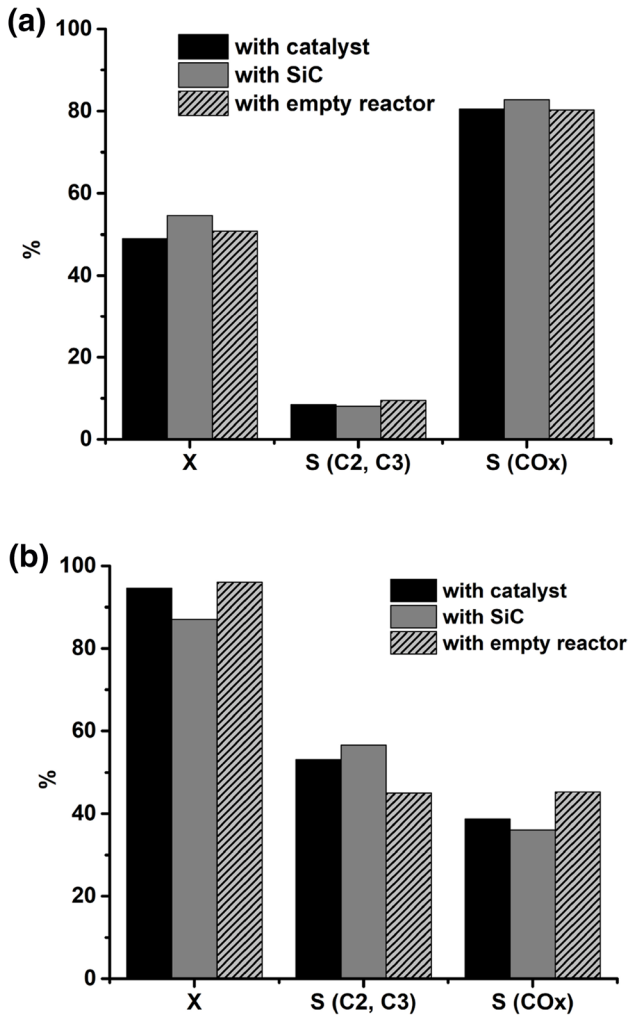

Fig. 6 Comparison of the reaction performance of **a** C_2H_4, **b** C_2H_6 in the presence of Mn–Na_2WO_4 catalyst, inert SiC material or empty reactor

conducted in the empty reactor could be explained by taking the gas phase reactions into consideration.

It should be noted that the gas phase reactions are mainly occurring as radical chain reactions. First, the radicals are formed in the rate-limiting step (initiation). Then, they react with the stable components and form new radicals (propagation step). Finally, the radicals would be converted to stable species in the termination step [58]. The interaction of these reactions establishes a steady state situation with a constant concentration of radicals in a radical pool. Therefore, it is expected that the concentration of the radicals would have a strong effect on the level of the conversion of the gas phase reactions. In the presence of the catalyst, a part of the radicals is quenched on the catalyst surface. Under these circumstances, less reactant can be activated during the reaction and this consequently results in a lower level of conversion, as observed in our studies.

The higher selectivity of the reaction observed in the presence of the catalyst is also consistent with our interpretations of the reaction mechanism of C_2 components. In the catalytic tests, a part of the oxygen was adsorbed on the surface of the catalyst. This resulted in a decrease in the concentration of the gas phase oxygen in the reactor. If the secondary oxidation of C_2 components is considered as reactions which mainly take place in the presence of the molecular O_2, then the lower rate of formation of CO_X would be an expected consequence.

This observation which was also reported earlier [40, 55], clearly shows the high influence of the gas phase reactions on the consecutive reaction of C_2 components. A difference between the nature of the gas phase conversion of ethane and ethene was also noticed when the results of these experiments were considered alongside the TPSR studies. The contribution of the homogeneous and heterogeneous reactions to the conversion of ethene is observed to change with the presence of oxygen in the reactor. However, ethane is shown to react mainly through the non-catalytic dehydrogenation reaction and the oxygen doesn't have a strong influence on the rate of this conversion. However, it can shift the equilibrium forward by reacting with hydrogen, the product of TDH of ethane.

The last experimental approach to verify the gas phase nature of the consecutive reaction of ethane was made by measuring its kinetic parameters in the presence and absence of the catalyst. A formal kinetic model was used for these studies. For this, activation energy and the reaction order of oxygen were calculated.

The activation energy was measured by calculating the conversion of ethane at different temperatures while a constant reaction mixture was sent to the reactor. The reaction was studied at temperatures of 585, 600, 615 and 630 °C, in the presence of the catalyst and at 585, 600, 615, 630 and 645 °C in the presence of silicon carbide (blank experiment). The logarithmic rate of consumption of ethane was plotted vs. the inverse of the reaction temperature (see SI, Figure S12). The slope of these curves is a function of the activation energy of the reaction as presented in Eq. (6). These results indicate that activation energy of ethane in the presence of catalyst is lower (256 KJ/mol) than in the presence of inert material, Si C (285 KJ/mol), showing an important role of the catalyst in the overall reaction.

$$\text{Slope} = -E_a/R \tag{6}$$

The reaction order of oxygen was calculated in the presence of both the catalyst and silicon carbide at temperatures of 585, 600, 615 and 630 °C. To do so, the rate of conversion of ethane was studied at each temperature while the initial concentration of oxygen was changing. The oxygen flow varied between 0, 3, 4, 5, 6, 7 Nml/min by substituting the flow of helium with oxygen. Both the total flow and

ethane flow were kept constant in the whole period of the studies. The rate of conversion of ethane at each of the tested temperatures was calculated. The results were depicted as a function of the oxygen concentration in a double logarithmic plot (see SI, Figures S13 and 14). The reaction order of oxygen in both conditions, in the presence of the catalyst or silicon carbide, was measured to be between 0.2 and 0.3 which is lower than the 0.5 reported in the literature [13, 51]. This observation indicates the low dependency of the reaction rate of ethane to the oxygen concentration at low conversions.

The similarity of the activation energy of ethane in addition to the low reaction order of oxygen in the blank and catalytic studies are in good agreement with the idea that the Mn_XO_Y–Na_2WO_4/SiO_2 has a negligible effect on the conversion of ethane under the applied reaction conditions.

Finally, the conversion of C_2 components under the co-feeding reaction conditions was simulated with Chemkin-Pro. The simulation was done using the Dooley mechanism. The reaction conditions applied to conduct the simulation were the same as those used in the co-feeding studies. The reaction was defined to occur in a plug flow reactor with the same dimensions as the experimental reactor. It was assumed that the reactor works in an isothermal situation. The temperature profile along the reactor, when the oven temperature was set at 750 °C, was measured and the obtained profile was exported to Chemkin to simulate the reaction behavior. The reaction mixture was defined as the mixture of 70 Nml/min of O_2/C_2H_6/He at a ratio of 1/1/33. The concentration profile of the components along the whole length of the reactor was calculated by the model. The concentration of the main products of the reaction, i.e. C_2H_X, CO_X, and H_2 at the reactor output were compared with the same values obtained during the experiment, see Fig. 7. As expected, the Dooley gas phase microkinetic model could predict the reaction behaviour of ethane and ethene well. The most noticeable deviation between the experimental and simulation results is related to the concentration of H_2 (not shown in Fig. 7). The reason for this observation is assigned to the fact that the Dooley mechanism doesn´t consider the decomposition reaction. This leads to an overestimation of ethene and simultaneously the underestimation of H_2 concentration predicted by the model.

4.2 Isotope-Labelled Experiments

So far, the reaction mechanism of C_2 components was investigated in the absence of the most abundant hydrocarbon in the OCM reactor, i.e. methane. Under these circumstances, the concentration of methyl radicals in the reactor is low. Therefore, it can be argued that the reaction mechanism of C_2 components obtained from our studies does not indicate the behavior of these compounds during OCM. The effect of partial pressure of methane on the consecutive reaction of C_2 components is already studied briefly [39, 40, 59, 60]. Unfortunately, the investigations over Mn_XO_Y–Na_2WO_4/SiO_2 were performed without isotope labelled hydrocarbons [39], that could lead to inaccurate interpretation due to the applied experimental procedure. In those studies, only the partial pressure of CH_4 was changed in a mixture of C_2, O_2, and N_2. The conversion of each of the hydrocarbons was calculated by comparing their concentration in the feed stream with that measured after the reaction. A decrease in the conversion of ethane and ethene was reported when the partial pressure of methane was increasing [39]. However, the occurrence of methane coupling reaction is not considered in that analysis. By increasing the concentration of methane in the reactor, the rate of conversion of methane to C_2 products has been enhanced. This automatically results in a higher concentration of C_2 components measured in the reactor

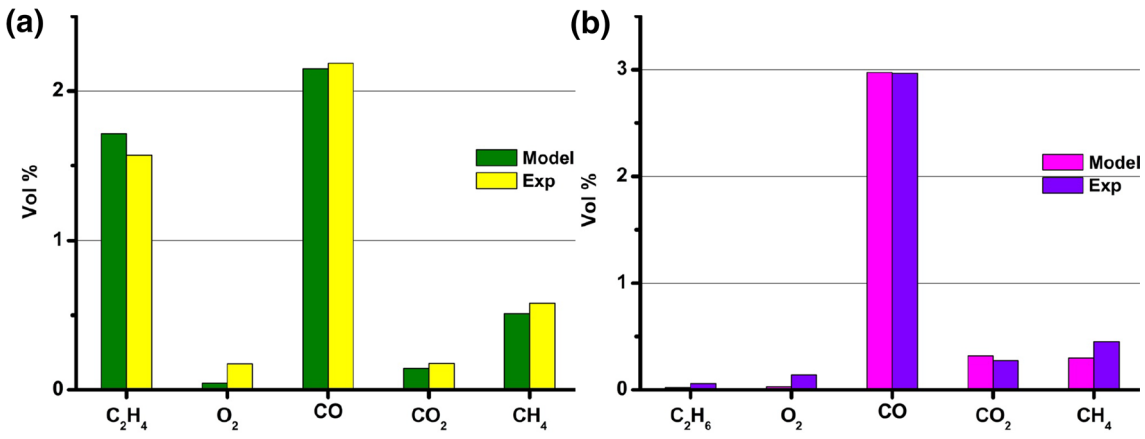

Fig. 7 Comparison of the concentration of the reaction products obtained experimentally with that calculated by Chemkin for the conversion of **a** ethane, **b** ethene

outlet. Since in the reaction mixture neither methane nor ethane were labelled, the authors could not distinguish the ethane formed from methane coupling reaction and the one introduced with the reaction mixture. To avoid the discussed misinterpretation, the same experiments were repeated in these studies using ^{13}C labelled methane.

The reaction of ethane in the co-feeding mode was investigated at a temperature of 700 °C. All the reaction conditions were constant except the partial pressure of the labelled methane in the feed. First, the reaction of ethane was tested by sending a flow of 3, 3 and 64 Nml/min of C_2H_6, O_2 and He to the reactor. Then, a flow of 5 Nml/min of labelled methane (^{13}C) was added to the reaction mixture. To keep the residence time constant, methane was substituted by the same flow of inert gas. The effluent was continuously analyzed by a semi GC–MS.

The changes in the I.In of CO_X, C_2H_4, C_2H_6 in the effluent was the determining parameter in these studies. Each of these components was detected by mass spectrometer at different time intervals. The labelled and non-labelled forms of the species were distinguished from each other by measuring their individual ionic masses as reported in Table 1. The results obtained from these measurements are presented in Fig. 8.

As it is shown in Fig. 8a, negligible changes were observed in the concentration of C_2H_6 in the presence and absence of the labelled methane ($^{13}CH_4$). This observation is consistent with the proposed gas phase nature for the conversion of ethane in the OCM reactor. However, the intensity of the ionic mass 25, assigned to the C_2H_4, was observed to increase slightly in the experiment performed in the presence of labelled methane, see Fig. 8a. It should be noted that the conversion of $^{13}CH_4$ results in the formation of both, labelled ethane (see Fig. 8e) and ethene (either $^{13}CH_2CH_2$ or $^{13}C_2H_4$, see Fig. 8f). The former product creates a peak at the ion mass of 25 similar to the normal ethene ($^{12}C_2H_4$). This suggests that the mentioned increase in the I.In of mass 25 observed in Fig. 8a is probably caused by measurement errors. Therefore, contrary to ethane, to draw a conclusion about the effect of methane on the behavior of ethene, more evidences are needed. This information is gained by comparing the rate of CO_X formation (presented in Fig. 8b–d). When the labelled methane was added to the reaction mixture, the rate of production of $^{12}CO_X$ decreased while the $^{13}CO_X$ was detected in the effluent. This observation indicates the consumption of a part of the surface oxygen by CH_4 as soon as it is introduced to the reactor (Fig. 8b, c). As discussed in the previous section, the heterogeneous reactions have a higher contribution to consecutive conversion of ethene than ethane. In addition, the conversion of ethene on the catalyst was shown to result in the formation of unselective products, either coke (from decomposition) or carbon oxidizes (if reacted with oxygen). In the presence of methane, the rate of oxidation of ethene is suppressed since there would be a competition between these two hydrocarbons to react with the surface oxygen species. These observations which are consistent with the literature reports, confirm the validity of the mechanistic modification suggested for consecutive reaction of C_2 components as discussed in the earlier section. The reasons for the influence of methane on the rate of secondary oxidation of these components reported in the earlier studies [39, 40, 59, 60] could also be explained by the competition for the surfaced bound oxygen.

Despite all these evidences confirming the gas phase nature of the consecutive reaction of ethane in the OCM reactor, it may be questioned how the Mn_XO_Y–Na_2WO_4 catalyst which can activate the more stable methane and ethene molecules has negligible influence on the conversion of ethane. This point is addressed in the last section of this study where the external mass transfer limitation is shown to be causing this behaviour.

4.3 Mass Transfer Condition in the Co-feeding Experiments

The concentration ratio of C_2 components and O_2 in the reaction mixture of the co-feeding experiments was chosen to simulate the real condition in the OCM reactor to a certain extent. Therefore, via calculating the Weisz–Prater (Ψ) and Mears (C_m) criterion [61, 62], valuable information regarding the mass transfer situation of methane, ethane, and ethene under OCM reaction conditions was obtained.

The Weisz–Prater criterion was calculated at 750 °C for each of the three co-feeding experiments (for the details of calculation see the supporting information). The value of Weisz–Prater in all the experiments was far smaller than one, see Table 3. Therefore, it is concluded that the rate of reaction of these components is not limited by any internal mass transfer limitation.

In the next step, the Mears criterion was calculated to study the external mass transfer situation in the performed experiments. Details of the calculation procedure are provided in the supporting information. For the reaction of methane, the parameter was much lower than 0.15, whereby in the reactions of ethane and ethene it exceeded this limit, i.e. 0.15, see Table 4. This observation indicated the influence of the external mass transfer on the reaction of C_2 components, especially ethane. This phenomenon was investigated for the reaction of ethane in more detail in a series of experiments. Conversion of ethane was tested in the co-feeding modus by keeping the feed composition constant (1/1/33 C_2H_6/O_2/He) while the total flow was increased from 70 to 140, 200, and 250 Nml/min. The conversion of ethane in each of these experiments was calculated and the results are presented in Fig. 9 as a function of the catalyst bed temperature. In the absence of mass transfer limitation, the rate

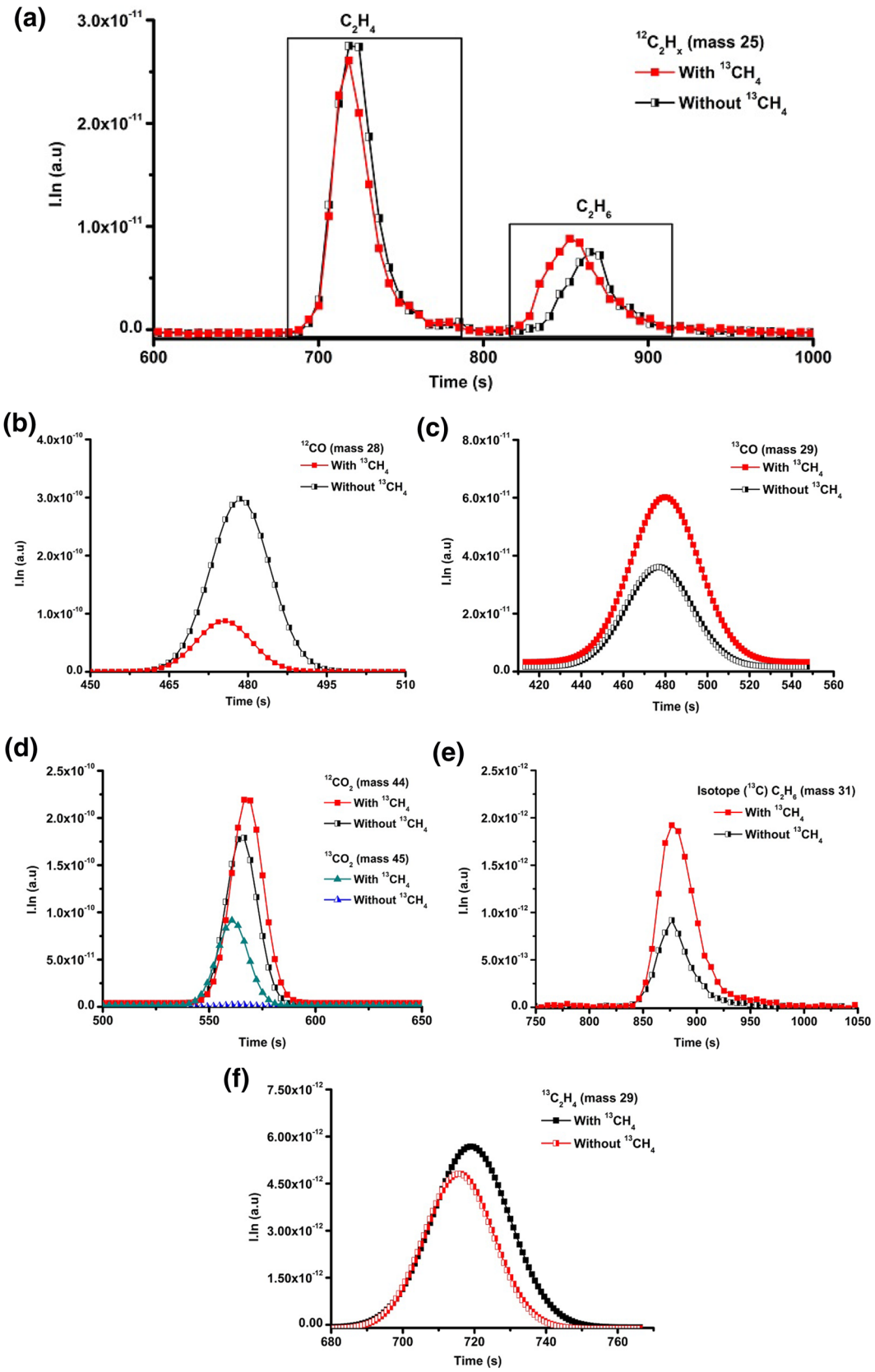

Fig. 8 Changes in the Ionic masses corresponding to the reaction products in the experiments done with (solid symbols), and without (the half-filled symbols), mixing CH_4 in the reaction mixture

Table 3 The calculated Weisz–Prater Criterion and the characteristic values implemented in calculating this criterion for each of CH_4, C_2H_6, and C_2H_4

	CH_4	C_2H_6	C_2H_4
Mean free path of the molecule, Λ (m)	1.5E−07	4.1E−08	7.7E−08
Diffusion coefficient in the free gas space, D_g (cm^2/s)	0.86	0.17	0.34
Initial concentration of the reactant, $C_{i,0}$ (mol/l)	1.6E−05	1.2E−06	1.2E−06
Reaction order, n	1	1	1
Effective diffusion coefficient, $D_{i,e}$ (cm^2/s)	0.09	0.02	0.03
Effective reaction rate at 775 °C, r_i (mol/(g·s))	3.7E−6	2.0E−05	3.3E−05
Weisz–Prater Criterion	1.2E−07	5.6E−05	1.7E−06

Table 4 The calculated Mears Criterion and the characteristic values implemented in calculating this criterion for each of CH_4, C_2H_6, and C_2H_4

	CH_4:O_2:He	C_2H_6:O_2:He	C_2H_4:O_2:He
Gas mixture ratio	4:1:5	1:1:33	1:1:33
υ_{mix} (m^2/s)	5.9E−05	9.99E−05	9.99E−05
Reynold Nr	0.25	0.15	0.15
Schmidt Nr	8.3	69.6	35.6
Sherwood Nr	2.6	2.9	2.8
k_c (m/s)	0.06	0.01	0.02
C_m	8.8E−04	0.59	0.15

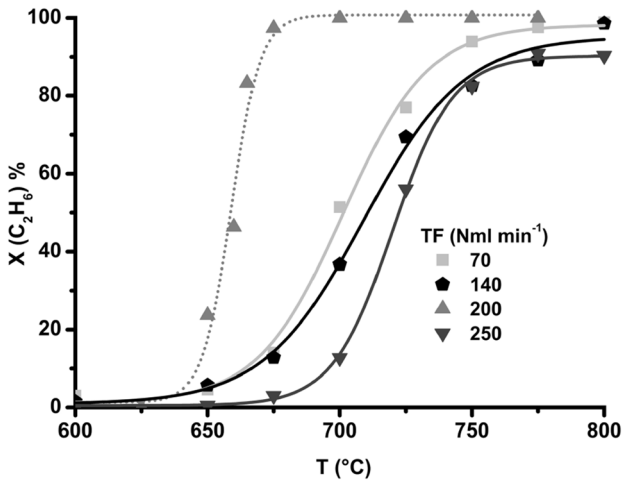

Fig. 9 Changes in the conversion of ethane in the co-feeding experiments performed at 70, 140, 200, 250 Nml/min total flow vs. temperature, reactant ratio: C_2H_6/O_2/He of 1/1/33, catalyst amount: 1 g

of conversion is expected to decrease at lower residence times. However, in our experiments, no direct correlation was seen between these two parameters, see Fig. 9.

First, the conversion of ethane decreased when the flow was raised from 70 to 140 Nml/min. This observation indicates that in this experiment, the residence time is the only parameter that controlles the reaction performance. But, as the flow was further raised to 200 Nml/min an increase in the conversion was observed. This behavior is assigned to the destruction of the diffusion layer surrounding the catalyst particles which allows ethane to reach the surface more easily. The increase made in the reaction rate under these circumstances has been so high that it has compensated the negative effect of the residence time. Therefore, a higher conversion was recorded for the reaction at the end. After this point, the most important parameter, influencing the reaction rate, should be the residence time again. This was also observed when a lower conversion of ethane was obtained by further increasing the flow rate to 250 Nml/min, see Fig. 9.

Based on the theoretical suggestion made by the Mears criteriams which were also proven experimentally (as discussed earlier), it was concluded that the consecutive reaction of ethane and ethene can be limited by the film diffusion under the OCM reaction conditions. Film diffusion limit also explains the results of our mechanistic studies,where it was shown that the conversion of ethane and ethene would mainly take place in the gas phase.

It worth mentioning that the selectivity of the reaction in the experiment done without the film diffusion limition (TF 200 Nml/min) was observed to be substantially lower compared to the one with film diffusion limition. (TF 70 Nml/min) (SI, Figure S15). This behavior is consistent with the high tendency of C_2 components to react through unselective oxidation or decomposition reactions over the catalyst surface as discussed earlier. This behavior indicates the possibility of controlling the reaction performance by adjusting the formation of diffusion layer as discussed in the following paragraph.

As it was mentioned earlier, when no layer is surrounding the catalyst, the rate of secondary conversion of C_2 components increased. This behavior shows that the presence of the film enhances the selectivity of the reaction. Thankfully, the mechanistic features of OCM enable to take advantage of the film diffusion limit to also enhance the performance of the reaction.

There is a conscience that the formation of ethane during OCM occurs by the coupling of methyl radicals in the gas phase of the reactor [3, 6, 17, 52, 63–65]. When the catalyst is covered with a film of an optimal thickness, methane can

diffuse through the film and form methyl radicals. The latter diffuse out of the film as easy as methane. Methyl radicals go through the coupling reaction to form ethane which can react further to form ethene. The cross-section area of C_2 components are almost twice as big as both methane and methyl radicals. Therefore, their transportation is limited along the diffusion layer. Under this circumstance the diffusion film would inhibit ethane and ethene from the consecutive reaction over the catalyst surface. It is therefore emphasized that the diffusion layer should not be too thick, otherwise it would prevent the diffusion of methane and methyl radicals. Accordingly, it is concluded that an optimized particle size, which gives the best influence of the diffusion film, can improve the performance of OCM.

5 Conclusions

The results of these studies indicated that the Mn_xO_y–Na_2WO_4/SiO_2 catalyst has a negligible effect on the consecutive dehydrogenation of ethane to ethene. The reason for this behavior is the external mass transfer limitation caused by the film surrounding the catalyst particles. The mass transfer limitation has shown to have a positive effect on the selectivity of the reaction to C_2 products. Under these conditions, the contact between the catalyst and both, ethene and ethane is reduced. Therefore, the rate of over-oxidation and decomposition of these components on the surface decreases.

The mechanistic investigations have shown that under the OCM reaction conditions the TDH rather than ODH reaction is the main route for converting ethane to ethene. Despite the complex mechanism of the OCM, the formation of CO_X is observed to be the result of over-oxidation of all the three main hydrocarbons of OCM, i.e. methane, ethane, and ethene. The secondary oxidation of C_2 components is observed to take place in the presence of gas phase oxygen. Therefore, it is concluded that regardless of the applied catalyst, suppression of oxygen from the homogeneous part of the reactor diminishes the formation of CO_X. Accordingly, implementing reactor concepts like chemical looping or membrane reactor, which fulfills this requirement, can be a promising solution for enhancing the performance of the OCM reaction.

Acknowledgements Financial support by the DFG (Grant No. EXC 314) (UniCat Cluster of Excellence) is gratefully acknowledged.

References

1. Lunsford JH (2000) Catalytic conversion of methane to more useful chemicals and fuels: a challenge for the 21st century. Catal Today 63:165–174. https://doi.org/10.1016/S0920-5861(00)00456-9
2. Malekzadeh A, Abedini M, Khodadadi A (2002) Critical influence of Mn on low-temperature catalytic activity of $Mn/Na_2WO_4/SiO_2$ catalyst for oxidative coupling of methane. Catal Lett 84:45–51
3. Arndt S, Otremba T, Simon U, Yildiz M, Schubert H, Schomäcker R (2012) $Mn–Na_2WO_4/SiO_2$ as catalyst for the oxidative coupling of methane. What is really known? Appl Catal A. https://doi.org/10.1016/j.apcata.2012.02.046
4. Lunsford JH (1990) Catalytic conversion of methane to heigher hydrocarbons. Catal Today 6:235–259. https://doi.org/10.1016/0920-5861(90)85004-8
5. Sinev MY, Fattakhova ZT, Lomonosov VI, Gordienko YA (2009) Kinetics of oxidative coupling of methane: bridging the gap between comprehension and description. J Nat Gas Chem 18:273–287. https://doi.org/10.1016/S1003-9953(08)60128-0
6. Kondratenko EV, Peppel T, Seeburg D, Kondratenko V, Kalevaru N, Martin A, Wohlrab S (2017) Methane conversion into different hydrocarbons or oxygenates: current status and future perspectives in catalyst development and reactor operation. Catal Sci Technol 7:366–381. https://doi.org/10.1039/C6CY01879C
7. Schwarz H (2011) Chemistry with methane: concepts rather than recipes. Angew Chemie 50:10096–10115. https://doi.org/10.1002/anie.201006424
8. Lunsford JH (1995) The catalytic oxidative coupling of methane. Angew Chemie 34:970–980. https://doi.org/10.1002/anie.199509701
9. Gesser HD, Hunter NR (1998) A review of C-1 conversion chemistry. Catal Today 42:183–189. https://doi.org/10.1016/S0920-5861(98)00090-X
10. Yildiz M, Aksu Y, Simon U, Kailasam K, Goerke O, Schomäcker R, Thomas A, Arndt S (2014) Enhanced catalytic performance of $MnxOy-Na_2WO\_SiO_2$ for the oxidative coupling. Chem Commun 50:14440–14442. https://doi.org/10.1016/j.apcata.2012.02.046
11. Shi C, Rosynek MP, Lunsford JH (1994) Origin of carbon oxides during the oxidative coupling of methane. J Phys Chem 98:8371–8376. https://doi.org/10.1021/j100085a017
12. Keller GE, Bhasin MM (1982) Synthesis of ethylene via oxidative coupling of methane I. Determination of active catalysts. J Catal 73:9–19. https://doi.org/10.1016/0021-9517(82)90075-6
13. Takanabe K, Iglesia E (2009) Mechanistic aspects and reaction pathways for oxidative coupling of methane on $Mn/Na_2WO_4/SiO_2$ catalysts. J Phys Chem C 113:10131–10145. https://doi.org/10.1021/jp9001302
14. Takanabe K, Iglesia E (2008) Rate and selectivity enhancements mediated by OH radicals in the oxidative coupling of methane catalyzed by $Mn/Na_2WO_4/SiO_2$. Angew Chemie 47:7689–7693. https://doi.org/10.1002/anie.200802608
15. Thybaut JW, Sun J, Olivier L, Van Veen AC, Mirodatos C, Marin GB (2011) Catalyst design based on microkinetic models: oxidative coupling of methane. Catal Today 159:29–36. https://doi.org/10.1016/j.cattod.2010.09.002
16. Yildiz M, Aksu Y, Simon U, Otremba T, Kailasam K, Göbel C, Girgsdies F, Görke O, Rosowski F, Thomas A, Schomäcker R, Arndt S (2016) Silica material variation for $MnxOy-Na_2WO_4/SiO_2$. Appl Catal A 525:168–179. https://doi.org/10.1016/j.apcata.2016.06.034
17. Lee MR, Park M, Jeon W, Choi J, Suh Y, Jin D (2012) A kinetic model for the oxidative coupling of methane over $Na_2WO_4/Mn/SiO_2$. Fuel Process Technol 96:175–182. https://doi.org/10.1016/j.fuproc.2011.12.038
18. Beck B, Fleischer V, Arndt S, Hevia MG, Urakawa A, Hugo P, Schomäcker R (2014) Oxidative coupling of methane—A complex surface/gas phase mechanism with strong impact on the reaction engineering. Catal Today 228:212–218. https://doi.org/10.1016/j.cattod.2013.11.059

19. Sinev MY (1992) Elementary steps of radical-surface interactions in oxidative coupling of methane. Catal Today 13:561–564. https://doi.org/10.1016/0920-5861(92)80081-W
20. Pak S, Qiu P, Lunsferd JH (1998) Elementary reactions in the oxidative coupling of methane over $Mn/Na_2WO_4/SiO_2$ and $Mn/Na_2WO_4/MgO$ Catalysts. J Catal 179:222–230
21. Ekstrom A, Lapszewicz Ja, Campbell I (1989) Origin of the low limits in the higher hydrocarbon yields in the oxidative coupling reaction of methane. Appl Catal 56:L29–L34. https://doi.org/10.1016/S0166-9834(00)80153-0
22. Nelson PF, Cant NW (1990) Oxidation of C2 hydrocarbon products during the oxidative coupling of methane over Li MgO. J Phys Chem 94:3756–3761
23. Parishana S, Littlewood P, Arinchtein A, Fleischer V, Schomäcker R (2017) Chemical looping as a reactor concept for the oxidative coupling of methane over the $MnxOy-Na_2WO_4/SiO_2$ catalyst, benefits and limitation. Catal Today. https://doi.org/10.1016/j.fuproc.2011.12.038
24. Zavyalova U, Holena M, Schlögl R, Baerns M (2011) Statistical analysis of past catalytic data on oxidative methane coupling for new insights into the composition of high-performance catalysts. ChemCatChem 3:1935–1947 https://doi.org/10.1002/cctc.201100186
25. Pak S, Lunsford JH (1998) Thermal effects during the oxidative coupling of methane over $Mn/Na_2WO_4/SiO_2$ and $Mn/Na_2WO_4/MgO$ catalysts. Appl Catal A 168:131–137
26. Palermo A, Pedro J, Vazquez H, Lee AF, Tikhov MS, Lambert RM (1998) Critical influence of the amorphous silica-to-cristobalite phase transition on the performance of $Mn/Na_2WO_4/SiO_2$ catalysts for the oxidative coupling of methane. J Catal 177:259–266
27. Wang D, Rosynek MP, Lunsford JH (1995) The effect of chloride ions on a Li + MgO catalyst for the oxidative dehydrogenation of ethane.pdf. J Catal 151:155–167
28. Fang X, Li S, Gu J, Yang D (1992) Preparation and characterization of W-Mn catalyst for oxidative coupling of methane. J Mol Catal 6:427–433
29. V. Fleischer, R. Steuer, S. Parishan, R. Schomäcker (2016) Investigation of the surface reaction network of the oxidative coupling of methane over Na < inf> 2</inf> WO < inf> 4</inf>/Mn/SiO < inf> 2</inf> catalyst by temperature programmed and dynamic experiments. J Catal. https://doi.org/10.1016/j.jcat.2016.06.014.
30. Yildiz M, Simon U, Otremba T, Aksu Y, Kailasam K, Thomas A, Schomäcker R, Arndt S (2014) Support material variation for the $MnxOy-Na_2WO_4/SiO_2$ catalyst. Catal Today 228:5–14. https://doi.org/10.1016/j.cattod.2013.12.024
31. Fleischer V, Steuer R, Parishan S, Schomäker R (2016) Investigation of the surface reaction network of the oxidative coupling of methane over $Na_2WO_4/Mn/SiO_2$ catalyst by temperature programmed and dynamic experiments. J Catal 341:91–103. https://doi.org/10.1016/j.jcat.2016.06.014
32. Le HV, Parishan S, Sagaltchik A, Goebel C, Schlesiger C, Malzer W, Trunschke A, Schomaecker R, Thomas A (2017) Solid-state ion-exchanged Cu/mordenite catalysts for the direct conversion of methane to methanol. ACS Catal. https://doi.org/10.1021/acscatal.6b02372
33. Arndt S, Simon U, Heitz S, Berthold a, Beck B, Görke O, Epping J-D, Otremba T, Aksu Y, Irran E, Laugel G, Driess M, Schubert H, Schomäcker R (2011) Li-doped MgO from different preparative routes for the oxidative coupling of methane. Top Catal 54:1266–1285. https://doi.org/10.1007/s11244-011-9749-z
34. Efstathiou aM, Verykios XE (1997) Transient methods in heterogeneous catalysis: experimental features and application to study mechanistic aspects of the CH_4/O_2 (OCM), NH_3/O_2 and NO/He reactions. Appl Catal A 151:109–166. https://doi.org/10.1016/S0926-860X(96)00262-1
35. Fleischer V, Littlewood P, Parishan S, Schomäcker R (2016) Chemical looping as reactor concept for the oxidative coupling of methane over a $Na_2WO_4/Mn/SiO_2$ catalyst. Chem Eng J 306:646–654. https://doi.org/10.1016/j.cej.2016.07.094
36. Dooley S, Dryer FL, Yang B, Wang J, Cool Ta, Kasper T, Hansen N (2011) An experimental and kinetic modeling study of methyl formate low-pressure flames. Combust Flame 158:732–741. https://doi.org/10.1016/j.combustflame.2010.11.003
37. Dooley S, Burke MP, Chaos M, Stein Y, Dryer FL, Zhukov VP, Finch O, Simmie JM, Curran HJ (2010) Methyl formate oxidation: speciation data, laminar burning velocities, ignition delay times, and a validated chemical kinetic model, Int J Chem Kinet. https://doi.org/10.1002/kin
38. Schwarz H, Geske M, Franklin Goldsmith C, Schlögl R, Horn R (2014) Fuel-rich methane oxidation in a high-pressure flow reactor studied by optical-fiber laser-induced fluorescence, multi-species sampling profile measurements and detailed kinetic simulations. Combust Flame 161:1688–1700. https://doi.org/10.1016/j.combustflame.2014.01.007
39. Lomonosov V, Usmanov T, Sinev M, Bychkov V (2014) Ethylene oxidation under conditions of the oxidative coupling of methane. Kinet Catal 55:474–480. https://doi.org/10.1134/S0023158414030070
40. Yu L, Li W, Ducarme V, Mirodatos C, Martin Ga (1998) Inhibition of gas-phase oxidation of ethylene in the oxidative conversion of methane and ethane over CaO, La_2O_3/CaO and $SrO–La_2O_3/CaO$ catalysts. Appl Catal A Gen 175:173–179. https://doi.org/10.1016/S0926-860X(98)00208-7
41. Roos JA, Korf SJ, Veehof RHJ, Van ommen JG, Ross JRH (1989) Reaction-path of the oxidative coupling of methane over a lithium-doped magnesium-oxide catalyst—factors affecting the rate of total oxidation of ethane and ethylene. Appl Catal 52:147–156. https://doi.org/10.1016/s0166-9834(00)83378-3
42. Sun J, Thybaut J, Marin G (2008) Microkinetics of methane oxidative coupling. Catal Today 137:90–102. https://doi.org/10.1016/j.cattod.2008.02.026
43. Falconer JL, Schwarz Ja (1983) Temperature-programmed desorption and reaction: applications to supported catalysts. Catal Rev 25:141–227. https://doi.org/10.1080/01614948308079666
44. Baró AM, Ibach H (1981) Thermal evolution and decomposition of ethylene on Pt(111). J Chem Phys 74:4194–4199. https://doi.org/10.1063/1.441549
45. Stroscio JA, Bare SR, Ho W (1984) The chemisorption and decomposition of ethylene and acetylene on Ni(110). Surf Sci 148:499–525. https://doi.org/10.1016/0039-6028(84)90596-X
46. Park C, Keane MA (2004) Catalyst support effects in the growth of structured carbon from the decomposition of ethylene over nickel. J Catal 221:386–399. https://doi.org/10.1016/j.jcat.2003.08.014
47. Haber J (2008) Fundamentals of hydrocarbon oxidation, Handb Heterog Catal. https://doi.org/10.1002/9783527610044.hetcat0170
48. Linic S, Barteau MA (2005) Heterogeneous catalysis of alkene epoxidation. Handb Heterog Catal. https://doi.org/10.1002/9783527610044.hetcat0175
49. Martin GA, Bates A, Ducarme V, Mirodatos C (1989) Oxidative conversion of methane and C2 hydrocarbons on oxides: homogeneous versus heterogeneous processes. Appl Catal 47:287–297. https://doi.org/10.1016/S0166-9834(00)83234-0
50. Asami K, Shikada T, Fujimoto K, Tominaga H (1987) Oxidative coupling of methane over lead oxide catalyst: kinetic study and reaction mechanism. Ind Eng Chem Res 26:2348–2353
51. Takanabe K, Shahid S (2016) Dehydrogenation of ethane to ethylene via radical pathways enhanced by alkali metal based catalyst in oxysteam condition. Aiche 63:3–194. https://doi.org/10.1002/aic.15447

52. Nelson PF, Lukey Ca, Cant NW (1988) Isotopic evidence for direct methyl coupling and ethane to ethylene conversion during partial oxidation of methane over lithium/magnesium oxide. J Phys Chem 92:6176–6179. https://doi.org/10.1021/j100333a003
53. Shahri SMK, Alavi SM (2009) Kinetic studies of the oxidative coupling of methane over the $Mn/Na_2WO_4/SiO_2$ catalyst. J Nat Gas Chem 18:25–34. https://doi.org/10.1016/S1003-9953(08)60079-1
54. Quiceno JWR, Deutschmann O (2005) Gas phase reactions: total and partial oxidation of C1-4 alkanes in the high and medium temperature range. Eur Combust Meet 64:1–41
55. Mims Ca, Mauti R, Dean aM, Rose KD (1994) Radical chemistry in methane oxidative coupling: tracing of ethylene secondary reactions with computer models and isotopes. J Phys Chem 98:13357–13372. https://doi.org/10.1021/j100101a041
56. Fleischer V, Simon U, Parishan S, Colmenares MG, Görke O, Gurlo A, Riedel W, Thum L, Schmidt J, Risse T, Dinse K-P, Schomäcker R (2018) Investigation of the role of the Na_2WO_4/Mn/SiO_2 catalyst composition in the oxidative coupling of methane by chemical looping experiments. J Catal 360:102–117
57. Kennedy EM, Cant NW (1991) Comparison of the oxidative dehydrogenation of ethane and oxidative coupling of methane over rare earth oxides. Appl Catal 75:321–330. https://doi.org/10.1016/S0166-9834(00)83141-3
58. Côme G-M (2001) Gas-phase thermal reactions: chemical engineering kinetics. Springer, Dordrecht. https://doi.org/10.1007/978-94-015-9805-7
59. Mackie JC, Smith JG, Nelson PF, Tyler RJ (1990) Inhibition of C2 oxidation by methane under oxidative coupling conditions. Energy Fuels 4:277–285. https://doi.org/10.1021/ef00021a011
60. Pogosyan NM, Pogosyan MD, Strekova LN, Tavadyan LA, Arutyunov VS (2015) Effect of the concentrations of methane and ethylene on the composition of the products of their cooxidation. Russ J Phys Chem B 9:218–222. https://doi.org/10.1134/S1990793115020104
61. Dittmeyer R, Emig G (2006) Simultaneous heat and mass transfer and chemical reaction. In: Ertl G, Knözinger H, Schüth F, Weitkamp J (eds) Handbook of heterogeneous catalysis. Wiley, Hoboken, pp 1727–1784. https://doi.org/10.1002/9783527610044.hetcat0094
62. Mohagheghi M, Bakeri G, Saeedizad M (2007) Study of the effects of external and internal diffusion on the propane dehydrogenation reaction over $Pt\text{-}Sn/Al_2O_3$ catalyst. Chem Eng Technol 30:1721–1725. https://doi.org/10.1002/ceat.200700157
63. Campbell KD, Morales E, Lunsford JH (1987) Gas-phase coupling of methyl radicals during the catalytic partial oxidation of methane. J Am Chem Soc 109:7900–7901. https://doi.org/10.1021/ja00259a059
64. Driscoll DJ, Martir W, Wang JX, Lunsford JH (1985) Formation of gas-phase methyl radicals over MgO. J Am Chem Soc 107:58–63. https://doi.org/10.1021/ja00287a011
65. Lee JS, Oyama ST (1988) Oxidative coupling of methane to higher hydrocarbons. Catal Rev 30:249–280. https://doi.org/10.1080/01614948808078620

Affiliations

Samira Parishan[1] · Ewa Nowicka[1] · Vinzenz Fleischer[1] · Christian Schulz[2] · Maria G. Colmenares[3] · Frank Rosowski[2] · Reinhard Schomäcker[1]

[1] Fachgebiet Technische Chemie, Institut für Chemie, Technische Universität Berlin, Straße des 17. Juni 124, 10623 Berlin, Germany

[2] BasCat - UniCat BASF Joint Lab, Technische Universität Berlin, Hardenbergstr. 36, 10623 Berlin, Germany

[3] Fachgebiet Keramische Werkstoffe/Chair of Advanced Ceramic Materials, Institut für Werkstoffwissenschaften und Technologien, Technische Universität Berlin, Hardenbergstraße 40, 10623 Berlin, Germany